Luminescence of Tm^{3+}, Yb^{3+} Co-doped $CaLaAlO_4/LaAlO_3$ Mixed Phase Phosphor for Solid-state Lighting Application

Victor Mshi IGBA [1], Marco Antonio GARCIA LOBATO [1], Carlos Eduardo RODRIGUEZ GARCIA [1, 2 *], Alejandro GARZA SANTIBÁÑEZ [3], Jorge OLIVA UC [4], Ernesto HERNÁNDEZ-HERNÁNDEZ [3], Efraín VIESCA-VILLANUEVA [1]

[1] *Facultad de Ciencias Químicas, Universidad Autónoma de Coahuila, Blvd. V. Carranza s/n esq. con Ing. José Cárdenas Valdés, Col. República Ote. C.P. 25280. Saltillo, Coahuila Mex*
[2] *Facultad de Ciencias Físico-Matemáticas, Universidad Autónoma de Coahuila, Edificio A Planta Alta, Unidad Camporredondo. C.P. 25020. Saltillo, Coahuila Mex*
[3] *Centro de Investigación en Química Aplicada, Enrique Reyna H. 140, San José de los Cerritos, 25294 Saltillo, Coahuila Mex*
[4] *Centro de Física Aplicada y Tecnología Avanzada de la UNAM, Campus UNAM 3001, 76230 Juriquilla Querétaro, México*

http://doi.org/10.5755/j02.ms.35356

Received 16 October 2023; accepted 24 December 2023

$CaLaAlO_4/LaAlO_3$: 0.5%Tm^{3+}, xYb^{3+} upconversion phosphors were prepared via the combustion method. The Tm^{3+} dopant concentration was constant (Tm=0.5mol%), while the concentration of Yb^{3+} co-dopant was varied (Yb = 1 – 10 mol%). The X-ray diffraction studies indicated a mixture of phases (tetragonal and hexagonal of $CaLaAlO_4$ and $LaAlO_3$ respectively). The optical absorption spectra of the upconversion phosphors have two absorption bands centered at 253 nm, and another band at 440 nm. The band at 253 nm is ascribed to the charge transfer band (CTB) between the ligand (O^{2-}) and Yb^{3+} ions, while the broad band located at 440 nm was related to defect states in the lattice. The energy bandgap and refractive index of the optimized phosphor were 4.73 eV and 1.76 respectively. The upconversion emission peaks centered at 478 nm ($^1G_4 \rightarrow {}^3H_6$), 654 nm ($^1G_4 \rightarrow {}^3F_4$), and 801 nm ($^3H_4 \rightarrow {}^3H_6$) are associated to the electronic transitions of Tm^{3+} ions. As the Yb concentration increases, the colour emission is tuned from bluish white to blue light. The CCT and CIE coordinate of (0.2419, 0.2463) showed that the phosphor doped with 10 mol% of Yb^{3+} produces a bluish-white and its colour purity was 80%. Thus, the strong bluish-white light emission produced by the $CaLaAlO_4/LaAlO_3$: 0.5%Tm^{3+}, xYb^{3+} phosphors could be used for solid-state lighting (SSL) or in multicolour displays.
Keywords: photoluminescence, up-conversion, bluish-white, phosphor, combustion synthesis.

1. INTRODUCTION

In the last century, many researchers have utilized rare earths (REs) in different host lattices as luminescent centers [1 – 3]. The inorganic luminescence material (phosphors) produced by doping with REs features a variety of electronic transitions within the 4f configuration [4]. These upconversion luminescence (UCL) materials find their applications in solid-state lighting (SSL) devices (light emitting diodes, luminescence lamps), plasma display panels, biological imaging, lasers, anticounterfeit, and solar cells [5, 6]. In comparison with traditional luminescence materials, UCL has low energy consumption, a long lifetime, and low excitation energy [7]. The RE-doped UCL materials can convert two or more low energy photons into one photon with higher energy in the visible region. Among the REs, Tm^{3+}, Er^{3+}, Eu^{3+}, Yb^{3+}, Ce^{3+}, and Dy^{3+} have been intensively researched [8 – 11]. Tm^{3+} ion is an efficient UCL center that has a narrow-line emission covering blue, red and NIR regions [12]. However, the luminescence efficiency of Tm^{3+} single doped host material is low [13]. This is because Tm^{3+} ions have many relaxation paths at the excited state. To enhance the UCL efficiency. Tm^{3+} ions can be co-doped with a sensitizer such as Yb^{3+} due to their closely matched intermediate-excited state [4]. Additionally, the absorption energy of Yb^{3+} matched well with the commonly used 980 nm laser diode for UCL [14]. Yb^{3+} is a good sensitizer that transfers the energy it absorbed to the activator [6, 7].

The host matrix has much influence on the luminescence properties of the dopants [5]. This is because it provides a platform for the energy transfer mechanism [7]. In this regard, efforts have been made to formulate a suitable host matrix that can effectively accommodate this configuration for efficient luminescence properties. Tm^{3+}/Yb^{3+} has been incorporated in different host matrices such as $BaLaAlO_4$ [15], $LaAlO_3$(16) Y_2O_3 [8] $Na_2Y_2B_2O_7$ [17], La_2O_3-TiO_2-ZrO_2 [18], $SrLaAlO_4$ [19], $ZrTi_{1.4}O_4$ [20], Ga_2O_3-Bi_2O_3-PbO [21] and $K_2Gd(PO_4)(WO_4)$ [12] phosphors for blue illumination. Also, these co-dopants are good and efficient luminescent centers with enhanced colour purity for SSL. $CaLaAlO_4$ phosphor has been scarcely researched. It belongs to a perovskite structure family $ABCO_4$, where A is a divalent cation, B and C are REs and transition metals, respectively [22]. This host matrix doped with REs provides excellent chemical and structural stability with efficient luminescent properties.

* Corresponding author. Tel.: +52-844-4148869; fax: +52-844-4144739.
E-mail: *crodriguezgarcia@uadec.edu.mx* (C.R. Garcia)

In this work, we reported the mixture of phases material $CaLaAlO_4/LaAlO_3$: 0.5 %Tm^{3+}, xYb^{3+} phosphors powders for the first time, at varying concentrations of Yb co-dopant concentration. The optical absorbance and energy bandgap of the pure and $CaLaAlO_4/LaAlO_3$: 0.5%Tm^{3+}, Yb^{3+} phosphor experimentally has also been determined for the first time. The UCL properties have been investigated in detail. It is found that the bluish-white emitting phosphor will have a potential application in SSL technology.

2. EXPERIMENTAL DETAILS

2.1. Synthesis of $CaLaAlO_4$-$LaAlO_3$: 0.5%Tm^{3+}, xYb^{3+} phosphors

$CaLaAlO_4/LaAlO_3$: 0.5 %Tm^{3+}, xYb^{3+} phosphors were prepared through a simple solution combustion method. The materials used were calcium nitrate tetrahydrate [$Ca(NO_3)_2$ $4H_2O$ (99.0 %)], lanthanum nitrate hexahydrate [$La(NO_3)_3$ $6H_2O$ (99.9 %)], aluminium nitrate nonahydrate [$Al(NO_3)_3$ $9H_2O$ (99.999 %)], urea [$CO(NH_2)_2$ (99.5 %)], thulium nitrate pentahydrate [$Tm(NO_3)_3$ $5H_2O$ (99.9 %)] and ytterbium nitrate pentahydrate [$Yb(NO_3)_3$ $5H_2O$ (99.999 %)]. The reagents used were of analytical grade. To prepare the phosphors, the stoichiometric amounts of all the oxidants together with urea were dissolved in double deionized (DI) water and a magnetic stirrer was used to stir the solution for about 30 minutes. After which the entire mixture was transferred into the heating furnace at 620 °C. During the heating process, the oxidants react explosively with an organic fuel (urea), and inflammable gases such as CO_2, NH_3 and NO_2 are produced [23], leaving behind the fluffy product.

The fluffy product (As-synthesized) formed was ground in an agar mortar into a fine powder and pressed into pellets. The pellets were then annealed at 1080 °C for 6 hours in air to obtain a crystalline phosphor. Throughout the synthesis, the amount of Tm was fixed (Tm = 0.5 mol%), while the Yb amount was varied (x = 0, 1, 3, 5, 7, and 10 mol%). The obtained samples were ground, packaged, and labelled as CLAO, CLAO 0, CLAO 3, CLAO 5, CLAO 7 and CLAO 10 respectively. The co-doped samples such as CLAO: Tm, Yb phosphors were named as $CaLaAlO_4/LaAlO_3$: 0.5 %Tm^{3+}, xYb^{3+}.

2.2. Characterization of $CaLaAlO_4/LaAlO_3$: 0.5%Tm^{3+}, xYb^{3+} phosphors

The crystalline phase of the synthesized CLAO: Tm, Yb phosphors was identified by using X-ray diffraction. We use Cu_Kα radiation (λ = 1.5406Å) on an X-ray diffractometer (Bruker, Advance D8), and the data were collected over the 2θ angle in the range of 20° – 80° with the scanning speed of 2°/min. Scanning electron microscopy (SEM) was employed to analyse the morphological composition of the phosphors (JEOL ARM200F, Peabody, MA, USA). Fourier Transform Infrared (FTIR) data was obtained by IRTracer-100, which was used to identify the IR absorptions in the phosphors. The optical absorbance spectra of the pure and CLAO: Tm, Yb phosphors were obtained using a UV-Vis-NIR Spectrophotometer (Cary-5000 Agilent) in the wavelength range of 200 – 800 nm. The Up-conversion Luminescence (UCL) properties were measured at room temperature using an ocean optic Spectrometer USB 2000 under 980 nm laser diode excitation. All measurements were acquired at room temperature.

3. RESULTS AND DISCUSSION

3.1. Structural analysis and morphological characterization of CLAO: Tm, Yb

The crystallinity and structural effect of the co-dopants on the CLAO host matrix were investigated by applying XRD. Fig. 1 a presents the X-ray diffraction patterns of undoped and CLAO: Tm, Yb phosphors.

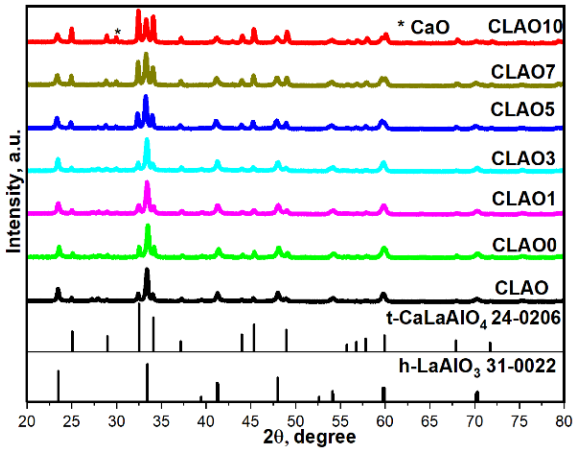

a

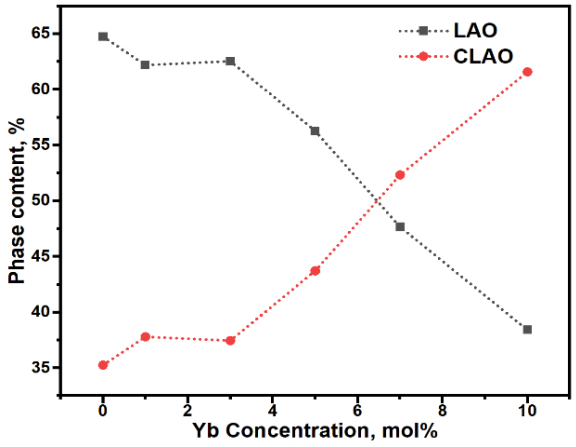

b

Fig. 1. a – The XRD pattern of CLAO: Tm, Yb; b – percentage of phase content in the samples as a function of Yb mol % co-dopant concentration

The diffraction peaks exhibit a mixed phase containing the tetragonal $CaLaAlO_4$ and the hexagonal $LaAlO_3$ structures. The peaks observed at 2θ values 24.968°, 32.422°, 34.055°, 37.282°, 45.266°, 48.962°, and 59.765° correspond to (101), (103), (110), (112), (114), (200), and (008) planes. Those are associated with the $CaLaAlO_4$ tetragonal phase according to the JCPDS card no. 24-0206. The patterns of the secondary phase showed reflections near 2θ angles of 23.457°, 33.402°, 41.284°, 48.023°, and 54.170°, which matched with the (012), (110), (006), (024), and (116) planes. Those are associated with the hexagonal $LaAlO_3$ perovskite according to the JCPDS No. 31-0022

card. The reason for the mixed phase in the phosphors could be the incomplete reactions of initial compounds and annealing time and temperature [24]. The peaks associated with the $LaAlO_3$ phase show a lower intensity with the Yb^{3+} concentration [11]. An impurity phase belonging to CaO was also observed (marked with an asterisk "*").

The crystallite sizes of the phosphor (tetragonal and hexagonal phases) were determined by taking the averages of the prominent and most symmetric peaks of each phase. The Debye Scherer's equation was employed (2).

$$D_{hkl} = \frac{k\lambda}{\beta_{hkl}\cos\theta_{hkl}}, \quad (2)$$

where D_{hkl} is the average crystallite size; λ symbolizes the Cu_Kα radiation wavelength (1.5406 Å); θ_{hkl} is the Bragg's angle (in radians); K refers to the shape factor ($k = 0.9$); β_{hkl} is the FWHM in radians. The calculated average crystallite sizes for the tetragonal phase are in the range of 20 to 27 nm, while those of the hexagonal phase are in the range of 20 to 25 nm. The percentage phase content (tetragonal $CaLaAlO_4$ and hexagonal $LaAlO_3$) was determined and presented in Fig. 1 b. As the Yb content increases, the $CaLaAlO_4$ phase becomes prominent, while that of $LaAlO_3$ gradually decreases. This result agrees well with the XRD pattern of the synthesized samples. It can be seen from the XRD pattern that, the increase in Yb content stabilizes the $CaLaAlO_4$ phase, whereas a decrease in the intensity of the $LaAlO_3$ perovskite phase was observed. This result suggests that more of the Tm^{3+}/Yb^{3+} ions preferentially occupy the $CaLaAlO_4$ phase than the $LaAlO_3$ perovskite structure, resulting to the decrease in the intensity of the hexagonal phase.

The site occupancy of Tm^{3+} and Yb^{3+} ions in the host crystal is determined by the ionic radii and the valence state [22]. Considering the charge similarity, Tm^{3+} and Yb^{3+} ions would prefer to occupy the La^{3+} site instead of the Ca^{2+} site. Therefore, the site occupancy can be determined using the radius percentage (R_r):

$$R_r = \frac{R_h(CN) - R_d(CN)}{R_h(CN)} \times 100\%, \quad (3)$$

where $R_h(CN)$ is the ionic radius of the host, while $R_d(CN)$ is the radius of the dopant, CN refers to the coordination number. For the tetragonal phase, $R_d(CN)$ in 8-coordination Tm^{3+} (1.052 Å) and Yb^{3+} (1.042 Å) substituted in the host cation La^{3+}(1.216 Å) [25]. Therefore, the value of R_r between the Tm^{3+} in the La^{3+} ions was determined as 13.49 %. On the other hand, the estimated value of R_r between the Yb^{3+} in La^{3+} cation site is 14.31 %. It is reported that the value of R_r should not be more than 15 % [19], therefore, Yb^{3+} and Tm^{3+} will conveniently be substituted in the La^{3+} cation site in the $CaLaAlO_4$ phase. Now, to estimate the site occupancy of Tm^{3+} (CN = 6; R_{Tm} = 0.880 Å) and Yb^{3+} (CN = 6; R_{Yb} = 0.868 Å) ions in the hexagonal perovskite structure. We consider the possible substitution of Tm and Yb in the La^{3+} (CN = 6; R_{La} = 1.032 Å) site. The estimated value of R_r of Tm^{3+} and Yb^{3+} in the La^{3+} cation site is 14.7 % and 15.9 % respectively. The percentage of Yb^{3+} in the La^{3+} cation site is slightly above the threshold value of 15 %. Many researchers consider 30 % as the threshold of the dopant substituting the host [26].

Fig. 2 represents the SEM micrographs of the synthesized samples at different Yb concentrations. The morphological composition, crystallinity and grain size of the phosphor have much influence on the photoluminescence. We also observed that the obtained particles showed agglomerated, have irregular shape and size distribution. There is no clear difference between the images. Most of the particles coalesce appearing to be agglomerate. The irregular size of the particles could be the uneven distribution of temperature during combustion.

3.2. FTIR analysis of the $CaLaAlO_4/LaAlO_3$: 0.5 %Tm^{3+}, Yb^{3+} phosphors

In Fig. 3 a, we showcase the FTIR spectrum of the as-synthesized material, representing the powder before annealing treatment for the CLAO sample. Notable absorption peaks at 3610 cm^{-1} 2170 cm^{-1}, 2029 cm^{-1}, 1415 cm^{-1}, 869 cm^{-1} and 724 cm^{-1} are observed, which are attributed respectively, to the vibrations OH-, C-C bond, N-O bond, and M-O bonds (with M = Al, La) [27 – 30].

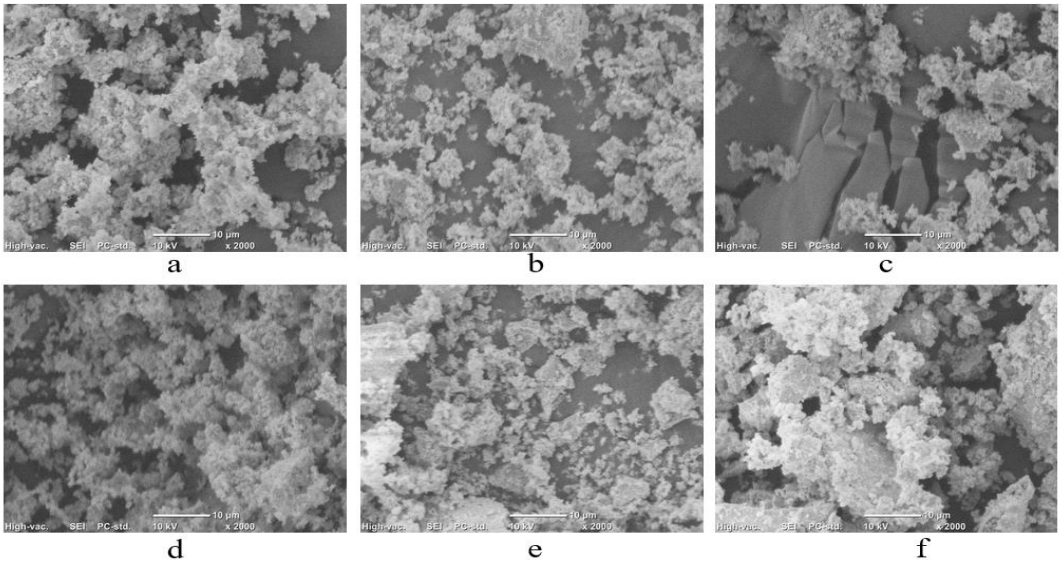

Fig. 2. The SEM micrographs: a – CLAO 0; b – CLAO 1; c – CLAO 3; d – CLAO 5; e – CLAO 7; f – CLAO 10 phosphors samples

Fig. 3 b shows the FTIR spectra of undoped and CLAO: Tm, Yb phosphors recorded in the range of 400 cm^{-1} – 4000 cm^{-1}. The FTIR is useful in determining the quenching centers of photoluminescence in phosphor materials.

It is worthy to note that the hydroxyl group enhances the non-radiative phenomenon in the upconversion luminescent materials. The sharp IR band at 3645 cm^{-1} is ascribed to the hydroxyl group (OH^-). This mode of vibration indicates the presence of water molecules in the samples. The hydroxyl group could quench the photoluminescence and reduce the emission efficiency of the phosphor [27]. The IR bands observed at 2029 cm^{-1} and 2170 cm^{-1} belong to the C-C bond. The broad peak observed at 1447 cm^{-1} belongs to the N-O vibration mode [28]. With the increment in Yb^{3+} contents, this band is shifted by 27 cm^{-1}. The IR absorption band observed at 443 cm^{-1} is due to the stretching and bending vibration of the Al-O bond in AlO_6 octahedron coordination. While the bands at 671, 717 and 878 cm^{-1} are assigned to the stretching vibrations of the La-O bond in the LaO_{12} dodecahedron [29]. The infrared absorption bands between 1000 cm^{-1} and 400 cm^{-1} belong to the metal-oxygen bond deformation mode [30]. These absorption bands are present in all the $CaLaAlO_4/LaAlO_3$ annealed samples.

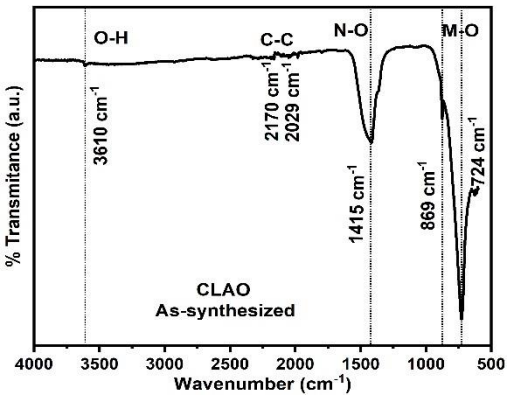

a

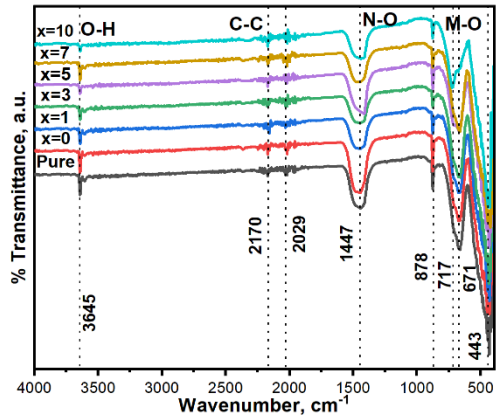

b

Fig. 3. a – FTIR spectrum of the as-synthesized sample CLAO before the annealing treatment; b – FTIR spectra of the CLAO pure (without co-dopants) and $CaLaAlO_4/LaAlO_3$: 0.5%Tm^{3+}, xYb^{3+} phosphors

3.2. Absorbance and optical bandgap of the pure and $CaLaAlO_4/LaAlO_3$: 0.5%Tm^{3+}, Yb^{3+} phosphors

Fig. 4 a presents the absorption spectra of pure and CLAO: Tm, Yb phosphors. We observed two absorption bands, one located at 253 nm and another at 440 nm.

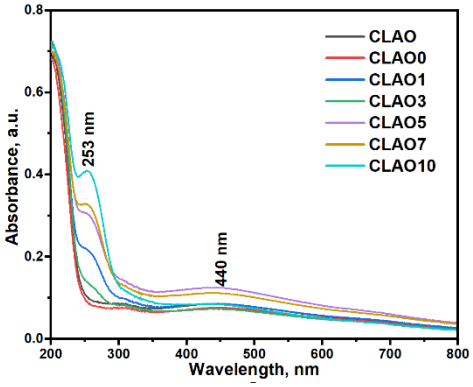

a

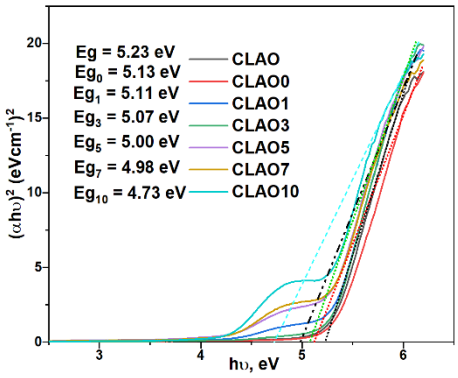

b

Fig. 4. a – Absorbance spectra of CLAO and CLAO: Tm, Yb phosphors; b – Tauc plot curves for the calculation of optical bandgap of pure CLAO and CLAO: Tm, Yb phosphors

The band at 440 nm is the broadband ascribed to defect states in the lattice [31]. The absorption peak at 253 nm is observed only in Yb-doped samples and can be ascribed to the charge transfer (CT) band between Yb^{3+} ions and the ligand O^{2-} atom (Yb – O) [32, 33]. Since the band is not broad, it means the change in the distance of Yb^{3+} ion and the ligand between the conduction band and the excited state is small, thus, the intermediate-coupling scheme was observed [34]. The optical bandgap for the phosphor was determined using Tauc's equation:

$$\alpha h\nu = A\left(h\nu - E_g\right)^n, \tag{4}$$

where A is called the proportionality constant; $h\nu$ and E_g refers to energies of the photon and bandgap, respectively, α refers to the absorption coefficient. The exponential value $'n'$ is the index which stands for direct allowed $\left(n = \frac{1}{2}\right)$, indirect allowed $(n = 2)$, direct forbidden $\left(n = \frac{3}{2}\right)$ and indirect forbidden $(n = 3)$ transitions, respectively. To determine the energy bandgap, a plot of $(\alpha h\nu)^{\frac{1}{n}}$ versus $(h\nu)$

was done, and the linear fit was extrapolated to the $(\alpha hv)^2 = 0$ on the energy axis see Fig. 4 b. The value of $'n'$ was determined by testing for direct and indirect allowed transitions. It was observed that, the increase in Yb concentration, decreases the energy bandgap of the material. The estimated energy bandgap for a pure sample and the CLAO: Tm, Yb phosphors decreases between 5.23 eV and 4.73 eV. This is evident that Yb^{3+} ions are substituted well in the host. The bandgap values indicate that the phosphor is an insulating material. To determine the refractive index of the phosphor, we used the relation [19]:

$$\frac{n^2-1}{n^2+1} = 1 - \sqrt{\frac{\varepsilon_g}{20}}, \quad (5)$$

where n is called the refractive index and ε_g is the optical bandgap of the phosphor. The refractive index was determined to be 1.706, 1.717, 1.719, 1.724, 1.732, 1.734, and 1.764 corresponding to CLAO, CLAO 0, CLAO 1, CLAO 3, CLAO 5, CLAO 7, and CLAO 10, respectively. We also noticed that n and Yb^{3+} concentration increases correspondingly. This increment enhances the photoluminescence properties [19].

3.3. Photoluminescence properties of $CaLaAlO_4/LaAlO_3$: 0.5%Tm^{3+}, xYb^{3+} phosphor

To investigate the luminescence properties of CLAO: Tm, Yb phosphor, the upconversion luminescence was performed. Fig. 5 a presents the upconversion emission spectra of CLAO: Tm, Yb phosphors, in the wavelength range of 400 nm to 900 nm. The spectra showed three emission bands centred at 478 nm (blue), 654 nm (red), and 801 nm (NIR). These emission peaks can be attributed to the $^1G_4 \rightarrow {}^3H_6$, $^1G_4 \rightarrow {}^3F_4$, and $^3H_4 \rightarrow {}^3H_6$ electronic transitions of Tm^{3+} ions, respectively [15, 19, 35]. It was observed that, the intensity of CLAO: Tm, Yb phosphor was very low both in the visible and the infrared region. To optimize the UC emission intensity, the Yb^{3+} concentration was varied (CLAO 0 to CLAO 10). From the spectra, we observed that as the concentrations of Yb increase (CLAO 0 to CLAO 7), the emission at the near-infrared region appears most intense followed by blue and then red emission in that order. At CLAO 10, the intensity of blue emission (478 nm) becomes prominent, whereas the red emission (654 nm) maintains its weak intensity value with an increasing trend. Grigorjevaite and Katelnikovas [12] observed a similar behaviour at varying Tm^{3+} ion contents. In general, increasing Yb^{3+} contents favor the UCL both in the visible and near infrared regions. It is worthy to note that quenching does not occur in the host crystals. This proves that quenching is solely dependent on the host matrix, the amount of dopants, and elevated temperature. Yang *et al* observed quenching at 20 mol% of Yb in Yb:YAG [36]. Similarly, $BaLaAlO_4$: Tm^{3+}, Yb^{3+} observed quenching at 6 mol% concentration of Yb^{3+} ions [15]). The prominent peak observed at 478 nm (blue) is due to energy transfer from the Yb^{3+} to Tm^{3+} ions [17]. The inset in Fig. 5 a shows the photograph of UC blue emission at CLAO 10. The percentage contributions of blue and red emissions were also calculated. The percentage contribution of blue emissions in the visible region ranges between 2.73 % and 39.75 % to the overall emissions. While the red emission has 2.43 % to 15.68 % contribution in the visible region. The effect of the sensitizer on the luminescence process was also studied, and a plot of the intensity against the Yb^{3+} ion concentration is presented in Fig. 5 b. As the concentration of Yb^{3+} increases, the emission intensity increases progressively. The continuous increase in the emission intensity can be attributed to the enhancement in the luminescence process.

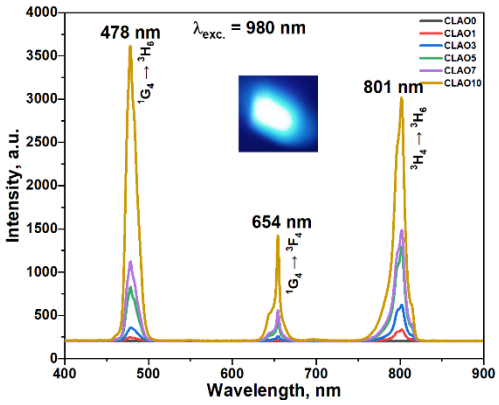

a

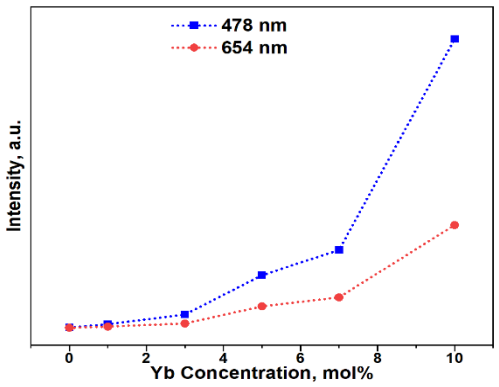

b

Fig. 5. a – The UCL emission spectra of CLAO: Tm, Yb phosphor; b – the plot of emission intensity versus Yb co-dopant concentrations

3.4. Commission internationale de l'éclairage (CIE) and colour map

Fig. 6 presents the CIE diagram obtained from UCL emission for the CLAO: Tm, Yb phosphor samples. The colour coordinates (CIE 1931) excited under a 980 nm laser diode are dependent on Yb^{3+} ion concentrations. The CIE values fall within the bluish white region, but gradually shift towards the blue region as the concentration of Yb increases. Thus, the prepared phosphor emits an efficient tunable emission from bluish white to blue light. The color emission is tuned toward the blue region due to the low contribution of red emission (16 % contribution to the overall visible emission). The CCT values are used to determine the light quality. It is established that the CCT values below 3200 K are considered warm light, while the values above 4200 K fall within the cool light region [37]. Then, we calculated the CCT values using the Mc Cammy equation [10]:

$$CCT = -437n^3 + 3601n^2 - 6861n + 5514.31, \quad (6)$$

where $n = (x-x_c)/(y-y_c)$, whereas $x_c = 0.332$ and $y_c = 0.186$ is the epicentre of iso-temperature. The calculated values of the CIE(x,y) chromaticity coordinates obtained from the CIE calculator at varying amounts of Yb^{3+} ions are presented in Table 1. It was observed that the values obtained from CCT are within the cool light source [10]. The color purity of the synthesized samples was also determined using the dominant wavelength (478 nm). The increase in Yb concentration increases the colour purity of the samples. The best colour purity for the sample was obtained as 79.76 % (see Table 1) as compared to the other Yb^{3+} doping concentrations. The high value of the colour purity means that the phosphor could be considered as an important component for white light emission diodes (WLED).

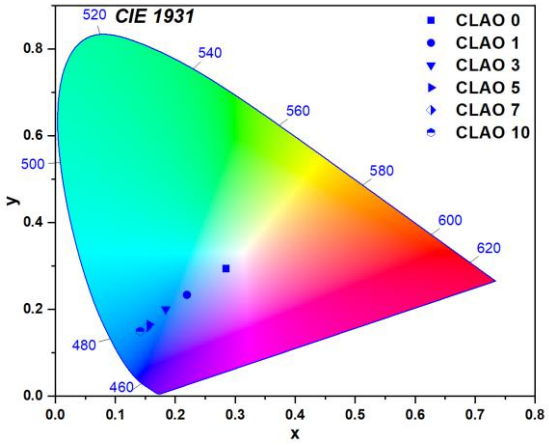

Fig. 6. CIE map for the CLAO: Tm, Yb phosphors under IR (980 nm) excitation

Table 1. The CIE coordinates for CLAO: Tm, Yb phosphors under IR excitation (980 nm)

Sample	CIE Coordinates		CCT, K	CP, %
	X	Y		
CLAO0	0.332316	0.333195	5278	9.25
CLAO1	0.330580	0.331596	5353	40.07
CLAO3	0.324838	0.326425	5618	57.70
CLAO5	0.306352	0.308266	6738	73.02
CLAO7	0.296201	0.298091	7605	74.46
CLAO10	0.241869	0.246335	22344	79.76

4. CONCLUSIONS

In summary, we have successfully synthesized Yb, Tm co-doped $CaLaAlO_4/LaAlO_3$ phosphor via solution combustion method and post annealing. The XRD results showed a mixture phase containing the tetragonal structure of $CaLaAlO_4$ and the hexagonal perovskite $LaAlO_3$ phase. The SEM micrographs showed agglomerated particles with irregular shape. The UCL properties of the phosphors were studied in the wavelength range of 400 nm to 900 nm at room temperature. The synthesized phosphor showed emission bands both in the visible and in NIR regions. A blue emission (478 nm) and NIR emission (801 nm) were observed to be intense, also a weak red emission (654 nm) of Tm^{3+} was also observed. The CCT and CIE coordinates (0.2419, 0.2463) showed that CLAO 10 (Yb = 10 mol%) produces a blue light (see, inset in Fig. 5 a) and its colour purity was 80 %. Thus, the strong bluish-white light emission produced by the CLAO: Tm, Yb phosphors could be used for potential applications in solid-state lighting or multicolour displays.

Acknowledgements

The authors acknowledge the National Council for humanity, Science and Technology (CONAHCyT) for the award of PhD scholarship to IGBA, VICTOR MSHI (No. 1241540). We are grateful for the support of Laboratorio Nacional en Innovación y Desarrollo de Materiales Ligeros para la Industria Automotriz (LANIAUTO) No. 321156 and Laboratorio Nacional de Materiales Grafenicos (LNMG) No. 321244. C.R. Garcia expresses gratitude to C. Mendez for insightful discussions.

REFERENCES

1. **Aroz, R., Lennikov, V., Cases, R., Luisa Sanjuán, M., de la Fuente, G.F., Muñoz, E.** Laser Synthesis and Luminescence Properties of $SrAl_2O_4$: Eu^{2+}, Dy^{3+} Phosphors *Journal of the European Ceramic Society* 32 (16) 2012: pp. 4363 – 4369. https://doi.org/10.1016/j.jeurceramsoc.2012.06.013
2. **Sehrawat, P., Khatkar, A., Boora, P., Khanagwal, J., Kumar, M., Malik, R.K., Khatkar, S.P., Taxak, V.B.** Tailoring the Tunable Luminescence from Novel Sm^{3+} Doped SLAO Nanomaterials for NUV-excited WLEDs *Chemical Physics Letters* 755 2020: pp 137758 – 137775. https://doi.org/10.1016/j.cplett.2020.137758
3. **Karbowiak, M., Rudowicz, C.** Crystal-field Analysis for RE^{3+} Ions in Laser Materials: I. Absorption Spectra and Energy Levels Calculations for Nd^{3+} and Pr^{3+} Ions in $ABCO_4$ Crystals *Chemical Physics* 383 (1 – 3) 2011: pp 68 – 82. https://doi.org/10.1016/j.chemphys.2011.04.008
4. **Wen, S., Zhou, J., Zheng, K., Bednarkiewicz, A., Liu, X., Jin, D.** Advances in Highly Doped Upconversion Nanoparticles *Nature Communications* 9 (1) 2018: pp. 2415 – 2427. https://doi.org/10.1038/s41467-018-04813-5
5. **Sehrawat, P., Khatkar, A., Boora, P., Kumar, M., Singh, S., Malik, R.K., Khatkar, S.P., Taxak, V.B.** Fabrication of Single-Phase $BaLaAlO_4$:Dy^{3+} Nanophosphors by Combustion Synthesis *Materials and Manufacturing Processes* 2020: pp. 1259 – 1267. https://doi.org/10.1080/10426914.2020.1762206
6. **Garcia, C.R., Oliva, J., Carranza, J., Mtz-Enriquez, A.I., Hdz-Garcia, H.M., Santibañez, A., Chavez, D.** Green Upconversion of a $SrLaAlO_4$: Yb, Er Phosphor and Its Application for LED Illumination *Journal of Electronic Materials* 52 (2) 2023: pp. 1357 – 1365. https://doi.org/10.1007/s11664-022-10091-1
7. **Chen, C., Li, C., Shi, Z.** Current Advances in Lanthanide-Doped Upconversion Nanostructures for Detection and Bioapplication *Advanced Science* 3 (10) 2016: pp. 1600029. https://doi.org/10.1002/advs.201600029
8. **Ryabochkina, P.A., Balashov, V.V., Volkova, T.V., Lyapin, A.A., Sidorova, N.V., Yurlov, I.A.** Nonradiative Energy Transfer Between Yb^{3+} and Tm^{3+} Ions in Y_2O_3:Tm, Yb Ceramics *Journal of Luminescence* 253 2023: pp. 119485. https://doi.org/10.1016/j.jlumin.2022.119485
9. **Laguta, V., Buryi, M., Pejchal, J., Uličná, K., Římal, V., Chlan, V., Stepankova, H., Zagorodniy, Y., Nilk, M.** Incorporation of the Ce^{3+} Activator Ions in $LaAlO_3$ Crystals:

EPR and NMR Study *Journal of Solid State Chemistry* 313 2022: pp. 123295.
https://doi.org/10.1016/j.jssc.2022.123295

10. **Shrivastava, R., Kaur, J., Dash, M.** Studies on White Light Emission of $Sr_2MgSi_2O_7$ Doped with Dy^{3+} Phosphors *Superlattices Microstructures* 82 2015: pp. 262 – 268.
https://doi.org/10.1016/j.spmi.2015.02.027
11. **Hasabeldaim, E.H.H., Swart, H.C., Kroon, R.E.** Luminescence, and Stability of Tb Doped CaF_2 Nanoparticles *Royal Society of Chemistry Advances* 13 (8) 2023: pp. 5353 – 5366.
https://doi.org/10.1039/D2RA07897J
12. **Grigorjevaite, J., Katelnikovas, A.** Optical Properties Investigation of Upconverting $K_2Gd(PO_4)(WO_4)$:20%Yb^{3+},Tm^{3+} Phosphors *Materials* 16 (3) 2023: pp. 1305.
https://doi.org/10.3390/ma16031305
13. **Shuai, P., Liao, L., Guo, Q., Yang, D., Shi, R., Mei, L.** Preparation and Up-conversion Luminescence Characteristics Studies of K_3YF_6: Ho^{3+}, Yb^{3+} with Cryolite Structure *Journal of Luminescence* 236 2021: pp. 118104.
https://doi.org/10.1016/j.jlumin.2021.118104
14. **Nair, G.B., Tamboli, S., Dhoble, S.J., Swart, H.C.** Conversion Phosphors: An Overview. In: Phosphor Handbook *Elsevier* 2023. pp. 73 – 98.
15. **Etafo, N.O., Oliva, J., Garcia, C.R., Mtz-Enríquez, A.I., Ruiz, J.I., Avalos-Belmontes, F., Lopez-Badillo, C.M., Gomez-Solis, C.** Enhancing of the Blue/NIR Emission of Novel $BaLaAlO_4$:Yb^{3+}(X mol%),Tm^{3+} (0.5 mol%) Upconversion Phosphors with the Yb^{3+} Concentration (X = 0.5 to 6) *Inorganic Chemistry Communications* 137 2022: pp. 109192.
https://doi.org/10.1016/j.inoche.2021.109192
16. **Jusza, A., Lipińska, L., Baran, M., Polis, P., Olszyna, A., Piramidowicz, R.** Short Wavelength Emission Properties of Tm^{3+} and Tm^{3+}+Yb^{3+} Doped $LaAlO_3$ Nanocrystals and Polymer Composites *Optical Materials (AMST)* 97 2019: pp. 109365.
https://doi.org/10.1016/j.optmat.2019.109365
17. **Soni, A.K., Dey, R., Rai, V.K.** Stark Sublevels in Tm^{3+}-Yb^{3+} Codoped $Na_2Y_2B_2O_7$ Nanophosphor for Multifunctional Applications *Royal Society of Chemistry Advances* 44 (5) 2015: pp. 34999 – 35009.
https://doi.org/10.1039/C4RA15891A
18. **Zhang, M., Liu, Y., Yu, H., Yu, J., Zheng, X., Ai, F., Pan, X., Zhao, H., Tang, M., Wen, H., Gai, L., Mao, Z., Wang, C.** Effect of Yb^{3+} on the Upconversion Luminescence of Tm^{3+}/Yb^{3+} Co-Doped La_2O_3-TiO_2-ZrO_2 Glasses *Optical Materials Express* 5 (4) 2015: pp. 676 – 683.
https://doi.org/10.1364/OME.5.000676
19. **Etafo, N.O., Garcia, R.C., Esquivel-Castro, T.A., León-Madrid, M.I., Santibañez, A., Oliva, J.** The Effect of a Yb Co-Dopant on the Blue Upconversion and Thermoluminescent Emission of $SrLaAlO_4$:Yb^{3+}, Tm^{3+} Phosphors *Coatings* 13 (6) 2023: pp. 1003.
https://doi.org/10.3390/coatings13061003
20. **Sangeetha, A., Hanumantharayappa, C., Nagabhushana, B.M., Jayasankar, C.K.** Tm^{3+} Doped, Yb^{3+} Sensitized Upconversion Photoluminescence and IR Emission in Zirconium Titanate Nano Composites *Optik (Stuttg)* 188 2019: pp. 40 – 45.
https://doi.org/10.1016/j.ijleo.2019.05.020
21. **Strzęp, A., Głowacki, M., Szatko, M., Potrząsaj, K., Lisiecki, R., Ryba-Romanowski, W.** Spectroscopic Properties of Thulium Doped $(Lu_{0.25}Gd_{0.75})_2SiO_5$ (LGSO) Single Crystals *Journal of Luminescence* 220 2020: pp. 116962.
https://doi.org/10.1016/j.jlumin.2019.116962
22. **Mendhe, M.S., Puppalwar, S.P., Dhoble, S.J.** Novel Single-Component $CaLaAlO_4$:Tb^{3+}, Eu^{3+} Phosphor for White Light-Emission *Optical Materials (AMST)* 82 2018: pp. 47 – 55.
https://doi.org/10.1016/j.optmat.2018.05.037
23. **Kadyan, S., Singh, S., Sheoran, S., Samantilleke, A., Mari, B., Singh, D.** Optical and Structural Investigations of $MLaAlO_4$:Eu^{3+} (M = Mg^{2+}, Ca^{2+}, Sr^{2+}, and Ba^{2+}) Nanophosphors for Full-Color Displays *Journal of Materials Science: Materials in Electronics* 31 (1) 2020: pp. 414 – 422.
https://doi.org/10.1007/s10854-019-02544-x
24. **Ankoj, P.I.** Structural Analysis of $CaLaAlO_4$ Powder via Solid State Method *International Journal in Research Applied Science and Engineering Technology* 6 (3) 2018: pp. 213 – 216.
https://doi.org/10.22214/ijraset.2018.3034
25. **Shannon, R.D.** Revised Effective Ionic Radii and Systematic Studies of Interatomic Distances in Halides and Chalcogenides *Acta Crystallographica Section A* 32 1976: pp. 751 – 767.
https://doi.org/10.1107/S0567739476001551
26. **Igba, V.M., Ahemen, I., Amah, A.N., Dejene, F.B., Sha'Ato, R., Reyes-Rojas, A., Duarte-Moller, J.A., Parra-Michel, J.R.** Structural Elucidation, and Optical Properties of $LiZrO_2$ –$LiBaZrO_3$ Nanocomposite Doped with Mn^{2+} Ions *Optical Materials Express* 10 (11) 2020: pp. 2877 – 2895.
https://doi.org/10.1364/OME.402111
27. **Han, K., Zhang, P., Wang, S., Guo, Y., Zhou, D., Yu, F.** Optical Characterization of Tm^{3+} Doped Bi_2O_3-GeO_2-Ga_2O_3 Glasses in Absence and Presence of BaF_2 *Scientific Reports* 6 2016: pp. 31207.
https://doi.org/10.1038/srep31207
28. **Kumari, A., Soni, A.K., Dey, R., Rai, V.K.** White Light Emission and Optical Heating in Er^{3+}-Tm^{3+}-Yb^{3+} Codoped La_2O_3 Phosphor *Journal of Display Technology* 12 (1) 2016: pp. 99 – 105.
https://doi.org/10.1109/JDT.2015.2457953
29. **Jana, P., Jayan, P.S., Mandal, S., Biswas, K.** Effect of Seeding on the Formation of Lanthanum Hexaaluminates Synthesized through Advanced Sol Gel Process *Journal of Crystal Growth* 208 2014: pp. 7 – 13.
https://doi.org/10.1016/j.jcrysgro.2014.09.015
30. **Mani, S., Rajamani, R., Ranjithkumar, B., Sathish, S., Nadaraj, D., Shankar, M., Dineshd, K.P.B., Ranjithkumare, R., Sengodanf, R., Rameshg, M., Shekar, B.C.** Structural and Electrical Properties of $LaAlO_3$ Nanoparticles *International Journal of Bioscience and Nanosciences* 1 (1) 2014: pp. 28 – 32.
31. **Jubu, P.R., Yam, F.K., Igba, V.M., Beh, K.P.** Tauc-Plot Scale and Extrapolation Effect on Bandgap Estimation from UV–Vis–NIR Data – A Case Study of β-Ga_2O_3 *Journal of Solid State Chemistry* 290 2020: pp. 121576.
https://doi.org/10.1016/j.jssc.2020.121576
32. **Van Pieterson, L., Heeroma, M., De Heer, E., Meijerink, A.** Charge Transfer Luminescence of Yb^{3+} *Journal of Luminescence* 91 (3 – 4) 2000: pp. 177 – 193.
https://doi.org/10.1016/S0022-2313(00)00214-3
33. **Khadiev, A., Akhmetov, N., Korableva, S., Morozov, O., Nizamutdinov, A., Semashko, V., Pudovkim, M., Gafurov, M.** The Impact of BiF_3 Doping on the Yb^{3+} to Yb^{2+} Reduction During the $LiYF_4$:Yb^{3+} Crystal-Growth Process *Ceramics* 5 (4) 2022: pp. 1198 – 206.

https://doi.org/10.3390/ceramics5040085

34. **Goud, K.M., Ramesh, C., Rao, A.** Spectroscopic Properties and Energy Transfer in Lead Bismuth Gallium Borate Glasses Codoped with Tm^{3+} and Yb^{3+} *International Journal of Research Engineering and Technology* 6 (1) 2017: pp. 215 – 220. https://doi.org/10.17577/IJERTV6IS010163

35. **Yang, P., Deng, P., Yin, Z.** Concentration Quenching in Yb:YAG *Journal of Luminescence* 97 2002: pp. 51 – 54.

36. **Sehrawat, P., Khatkar, A., Devi, S., Hooda, A., Singh, S., Malik, R.K.** An Effective Emission of Characteristic Cool White Light from Dy^{3+} Doped Perovskite Type $SrLa_2Al_2O_7$ Nanophosphors in Single-Phase pc WLEDs *Chemical Physics Letters* 737 2016: pp. 136842. https://doi.org/10.1016/j.cplett.2019.136842